Respiratory Research

RESEARCH

Open Access

Molecular mechanisms and therapeutic targets of acute exacerbations of chronic obstructive pulmonary disease with *Pseudomonas aeruginosa* infection

Zhiwei Lin[1,2], Shuang Liu[2], Ke Zhang[1], Tianyu Feng[1], Yewei Luo[3], Yu Liu[3], Baoqing Sun[2*] and Luqian Zhou[1*]

Abstract

Background Chronic Obstructive Pulmonary Disease (COPD) is a leading cause of global mortality, with acute exacerbations of COPD (AECOPD) significantly increasing the disease's morbidity and mortality. Among the pathogens implicated in AECOPD, *Pseudomonas aeruginosa* (*P. aeruginosa*) is increasingly recognized as a major co-infecting bacterium. Despite its clinical importance, the molecular mechanisms and therapeutic targets underlying AECOPD with *P. aeruginosa* infection remain inadequately understood.

Methods We employed a multi-omics approach, integrating proteomic analyses of bronchoalveolar lavage fluid (BALF) and plasma with transcriptomic analysis of peripheral blood. A discovery cohort of 40 AECOPD with *P. aeruginosa* infection patients and 20 healthy controls was analyzed, followed by validation in an independent cohort of 20 patients and 10 controls. Differentially expressed proteins (DEPs) and genes (DEGs) were identified and subjected to protein-protein interaction (PPI) network analysis, weighted gene co-expression network analysis (WGCNA), and immune infiltration analysis. Molecular docking simulations were conducted to explore potential therapeutic agents.

Results Our integrative analysis identified key biomarkers, which played critical roles in oxidative stress and neutrophil extracellular trap (NET) formation, both of which were pivotal in the pathogenesis of AECOPD with *P. aeruginosa* infection. The combined analysis of BALF, plasma, and peripheral blood underscored the interplay between local lung changes and systemic immune responses. Functional enrichment analyses highlighted significant pathways related to bacterial defense, inflammation, and immune activation. Validation in an independent cohort confirmed the diagnostic value of three key proteins (AZU1, MPO, and RETN), with high area under the curve (AUC) values in ROC analyses. Molecular docking indicated strong binding affinities of these proteins with Pioglitazone and Rosiglitazone, suggesting potential therapeutic utility.

Zhiwei Lin and Shuang Liu should be regarded as co-first authors.

*Correspondence:
Baoqing Sun
sunbaoqing@vip.163.com
Luqian Zhou
zhlx09@163.com

Full list of author information is available at the end of the article

Conclusions This study provides a comprehensive understanding of the molecular mechanisms underlying AECOPD with *P. aeruginosa* infection, highlighting the pivotal roles of oxidative stress and NET formation in disease progression. The identified biomarkers offer promising diagnostic and therapeutic targets. Our findings pave the way for novel strategies to improve outcomes for AECOPD patients with *P. aeruginosa* infection. While the study design limits our ability to establish causality, these results provide important insights that warrant further investigation, particularly through longitudinal studies, to confirm the specific contributions of *P. aeruginosa* in exacerbations.

Clinical trial number Not applicable.

Keywords AECOPD, *Pseudomonas aeruginosa*, Neutrophil extracellular traps, Oxidative stress, Biomarker, Therapeutic targets, Multi-Omics

Introduction

Chronic Obstructive Pulmonary Disease (COPD) is a prevalent respiratory condition projected to become the fourth leading cause of death globally by 2060, accounting for an estimated 5.4 million deaths annually [1]. COPD imposes a significant burden on healthcare systems and is associated with high rates of early mortality [2]. Patients who experience frequent exacerbations suffer from reduced quality of life, accelerated decline in lung function, as measured by forced expiratory volume in one second (FEV1), and increased mortality [3]. A history of previous exacerbations remains the strongest predictor of future episodes [4].

Acute exacerbations of COPD (AECOPD) are often complicated by respiratory infections, which can intensify inflammation and contribute to progressive airway damage [5]. A systematic review indicated that bacterial infections are present in approximately 50% of exacerbation cases [6]. However, current preventive strategies outlined in the GOLD guidelines are limited to one antibiotic, azithromycin, and two vaccines, leaving a significant gap in effective prophylactic therapies [1]. The complex interplay of factors that trigger exacerbations suggests that more comprehensive management strategies are needed [2].

Among the pathogens implicated in AECOPD, *Pseudomonas aeruginosa* (*P. aeruginosa*) is increasingly recognized as a major co-infecting bacterium [7]. Infections with *P. aeruginosa* are associated with increased morbidity and mortality, primarily due to extensive lung tissue damage, cell death, and a robust immune response [8]. Observational studies have shown that patients with declining lung function exhibit reduced lung microbiome diversity, with *P. aeruginosa* predominating in this group [9]. Despite extensive research, the pathogenic mechanisms underlying AECOPD with *P. aeruginosa* infection, particularly the complex interactions within the immune system, remain poorly understood. Additionally, the connection between local pulmonary pathogenesis and systemic immune responses, as reflected in peripheral blood pathways, has yet to be fully elucidated [9, 10]. Addressing these gaps is essential for developing more effective therapeutic strategies.

Neutrophils play a central role in the body's initial defense against bacterial infections [11], and airway neutrophilia is a characteristic feature of respiratory diseases, including COPD [12]. Neutrophil extracellular traps (NETs), composed of DNA, histones, and granule proteins, are crucial in trapping and neutralizing pathogens [13]. However, while NETs effectively immobilize pathogens, they can also exacerbate tissue damage and inflammation, complicating the pathology of bacterial pneumonias [14]. In the context of P. aeruginosa infections, NETs have been shown to contribute to the persistence and severity of the infection by inducing excessive inflammatory responses and promoting oxidative stress. Oxidative stress, resulting from an imbalance between reactive oxygen species (ROS) production and antioxidant defenses, further contributes to cellular damage and is pivotal in NET formation [15]. In AECOPD with *P. aeruginosa* infection, NETs and ROS are likely to play similarly significant roles, potentially causing harm rather than offering protection. However, this has yet to be investigated.

In this study, we aimed to elucidate the molecular mechanisms underlying AECOPD with *Pseudomonas aeruginosa* infection and to identify relevant biomarkers using a comprehensive multi-omics approach. We established a discovery cohort of 40 AECOPD with *P. aeruginosa* infection patients, along with 20 healthy controls, and a validation cohort comprising 20 patients and 10 controls. Using advanced proteomic analysis of bronchoalveolar lavage fluid (BALF) and plasma, alongside transcriptomic analysis of peripheral blood, we explored both local and systemic responses to AECOPD with *P. aeruginosa* infections. Our integrative analysis, including protein-protein interaction (PPI) networks, weighted gene co-expression network analysis (WGCNA), and immune infiltration analysis, identified critical pathways and molecular interactions involved in AECOPD with *P. aeruginosa* infection [16]. Based on these key targets, we employed the DSigDB database to predict potential therapeutic agents and performed molecular docking

to validate the binding efficiency of these drugs to key proteins [17]. This multi-omics approach offers a comprehensive view of the molecular mechanisms underlying AECOPD with *P. aeruginosa* infection and highlights potential targets for therapeutic intervention.

Methods

Study design and participant selection

This study was conducted with ethical approval from the Ethics Committee of The First Affiliated Hospital of Guangzhou Medical University (approval codes: 2022 No.121 and 2024 No. G-007). Written informed consent was obtained from all participants prior to enrollment.

Patients with AECOPD with *P. aeruginosa* infection were selected based on the 2024 Global Initiative for Chronic Obstructive Lung Disease (GOLD) definition of AECOPD, characterized by exacerbations with worsening respiratory symptoms, such as dyspnea, cough, or sputum production, within a 14-day period, with *P. aeruginosa* confirmed by bacterial culture. Patients experiencing mild to moderate exacerbations who were clinically stable enough to undergo bronchoscopy were included in the study. The exclusion criteria were as follows: (1) known respiratory disorders other than COPD; (2) history of lung surgery or tuberculosis; (3) cancer diagnosis; (4) recent blood transfusion (within four weeks of enrollment); (5) autoimmune diseases; (6) participation in a blinded drug trial; (7) antibiotic use within the past eight weeks; (8) endocrine disorders such as diabetes and connective tissue diseases; (9) other systemic inflammatory diseases; and (10) severe cardiovascular, cerebrovascular, hepatic, renal, or psychiatric disorders, or a history of pulmonary surgery. Healthy controls were recruited from a health examination center and screened to ensure the absence of chronic respiratory or other listed conditions.

Based on these criteria, 40 AECOPD with *P. aeruginosa* infection patients and 20 healthy controls were recruited as the discovery cohort between January 2023 and March 2024 from The First Affiliated Hospital of Guangzhou Medical University. Additionally, 20 AECOPD with *P. aeruginosa* infection patients and 10 healthy controls were recruited as the validation cohort. Comparative analyses between cohorts included assessments of demographic data, lung function (FEV1, FVC, FEV1/FVC), and inflammatory markers (WBC, NEU, LYM, MONO, EOS). All participants underwent bronchoscopy to obtain BALF samples for proteomic analysis, along with plasma proteomics and peripheral blood transcriptomics (Fig. 1). For details, see Supplementary Methods 1–3.

Liquid Chromatography-Mass spectrometry (LC-MS) analysis

For LC-MS analysis, 5 µL of each sample was first denatured using 8 M urea in 100 mM ammonium bicarbonate, bringing the final volume to 50 µL. Proteins were reduced with 10 mM dithiothreitol (DTT) at 37 °C for 30 min and

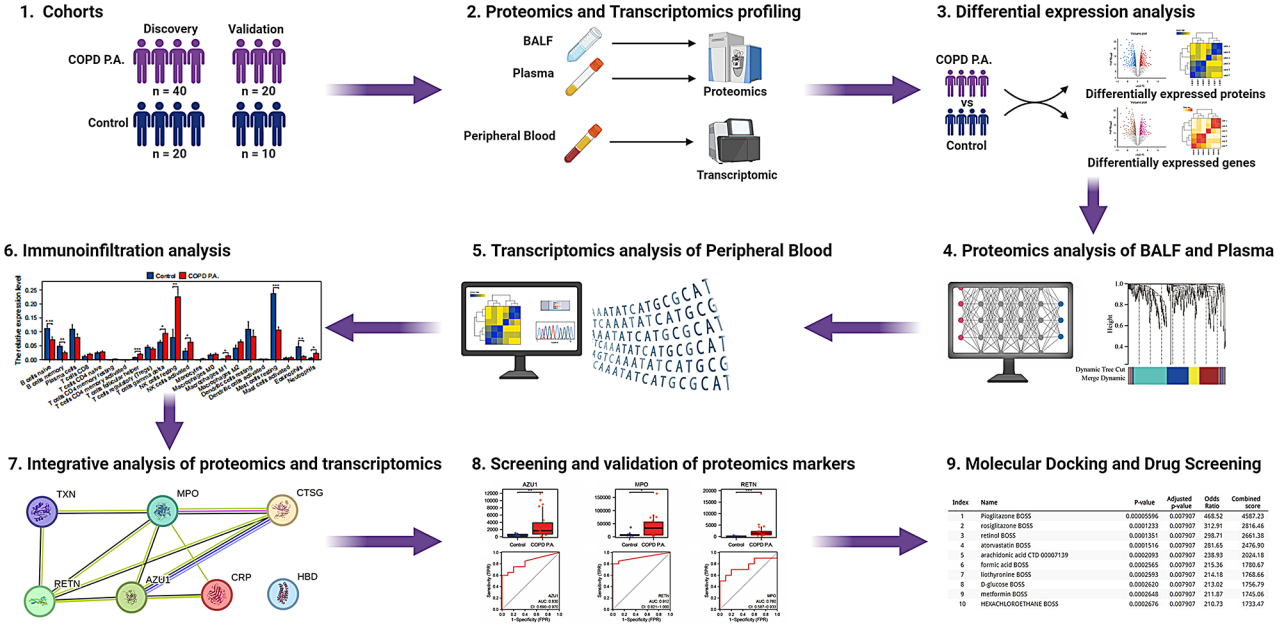

Index	Name	P-value	Adjusted p-value	Odds Ratio	Combined score
1	Pioglitazone BOSS	0.00005596	0.007907	468.52	4587.23
2	rosiglitazone BOSS	0.0001233	0.007907	312.91	2816.46
3	retinol BOSS	0.0001351	0.007907	298.71	2661.36
4	atorvastatin BOSS	0.0001516	0.007907	281.65	2476.90
5	arachidonic acid CTD 00007139	0.0002093	0.007907	238.93	2024.18
6	formic acid BOSS	0.0002565	0.007907	215.36	1780.67
7	liothyronine BOSS	0.0002593	0.007907	214.18	1768.66
8	D-glucose BOSS	0.0002620	0.007907	213.02	1756.79
9	metformin BOSS	0.0002648	0.007907	211.87	1745.06
10	HEXACHLOROETHANE BOSS	0.0002676	0.007907	210.73	1733.47

Fig. 1 Multi-Omics Analysis for AECOPD with *P. aeruginosa* infection. This study utilizes a two-stage design comprising an initial discovery cohort, which is subsequently validated in a separate cohort. We conducted proteomic analyses of bronchoalveolar lavage fluid and plasma samples, alongside transcriptomic profiling of peripheral blood samples. These analyses were followed by comprehensive bioinformatics investigations aimed at elucidating the underlying mechanisms and identifying biomarkers associated with -induced acute exacerbations of chronic obstructive pulmonary disease with *Pseudomonas aeruginosa* infection

subsequently alkylated with 50 mM iodoacetamide (IAA) in the dark at room temperature. The solution was then diluted with 50 mM ammonium bicarbonate, and trypsin (Promega, Madison, WI, USA) was added at a 1:30 enzyme-to-substrate ratio for overnight digestion at 37 °C. Following digestion, peptides were desalted using a C18 StageTip and quantified using a NanoDrop One spectrophotometer (Thermo Fisher Scientific, Waltham, MA, USA) at 280 nm.

The peptides were loaded onto a C18 reversed-phase column (15 cm length, 75 µm inner diameter, 2 µm particle size; Dr. Maisch GmbH, Ammerbuch, Germany) and eluted over 60 min with a gradient from 2 to 90% acetonitrile (ACN) in 0.1% formic acid (FA) at a flow rate of 300 nL/min. This gradient was optimized to ensure maximal peptide separation and identification.

Mass spectrometry acquisition was carried out on a timsTOF Pro2 (Bruker, Billerica, MA, USA) in Parallel Accumulation–Serial Fragmentation (PASEF) mode, utilizing the data-independent acquisition (DIA) diaPASEF method. The diaPASEF covered a mass-to-charge ratio (m/z) range of 400–1200 and an ion mobility range of 0.7 to 1.43 V·s/cm², employing a 32 × 25 Th window scheme with a ramp time of 100 ms. Data were processed using Spectronaut 18 (Biognosys AG, Schlieren, Switzerland) with a search conducted against the UniProtKB human protein database. The search parameters included trypsin as the enzyme, up to two missed cleavages, and mass tolerances set for precursor and fragment ions. Carbamidomethylation of cysteines was set as a fixed modification, while methionine oxidation and N-terminal acetylation were variable modifications. The interference correction for MS/MS scan was enabled. The database search results were filtered and exported with < 1% false discovery rate (FDR) at peptide-spectrum-matched level, and protein level, respectively [18]. After processing, a total of 592 valid proteins were identified, which were then subjected to further analysis. Normalization was achieved by equalizing medians at the peak group level [19]. For details, see Supplementary Methods 1.

RNA extraction, library preparation, and transcriptomic data processing

Total RNA was extracted using the TRIzol™ Reagent (Invitrogen, Carlsbad, CA, USA), and RNA purity was assessed with a NanoDrop spectrophotometer (Thermo Fisher Scientific, Waltham, MA, USA). RNA concentration was determined using the Qubit RNA BR (Broad-Range) Assay Kit (Thermo Fisher Scientific, Waltham, MA, USA), and RNA integrity was evaluated using RNA ScreenTape with the Agilent 4200 TapeStation (Agilent Technologies, Santa Clara, CA, USA). Depending on the total RNA yield, 0.1–1 µg of RNA was used for mRNA isolation, performed with the NEBNext® Poly(A) mRNA Magnetic Isolation Module (New England Biolabs, Ipswich, MA, USA). The mRNA libraries were then prepared using the NEBNext® Ultra™ II mRNA Library Prep Kit for Illumina® (New England Biolabs, Ipswich, MA, USA). After library preparation, the concentration of the libraries was measured using the Qubit™ dsDNA HS Assay Kit (Thermo Fisher Scientific, Waltham, MA, USA), and fragment size distribution was analyzed with the Agilent 4200 TapeStation and D1000 ScreenTape (Agilent Technologies, Santa Clara, CA, USA). Library molar concentration was determined using the KAPA Library Quant Kit for Illumina® Platforms (Roche, Basel, Switzerland). The libraries were sequenced on an Illumina NovaSeq 6000 system using the NovaSeq S4 reagent kit to generate paired-end reads.

Raw reads in FASTQ format were processed using fastp for quality control, including adapter trimming and filtering of low-quality reads. Reads were then aligned to the reference genome using HISAT2 v2.1.0 with default parameters. Gene quantification was performed using FeatureCounts, and TPM (Transcripts Per Million) values were calculated to normalize gene expression levels. A total of 20,504 valid RNAs were identified for further transcriptomic analysis. For quality control, see Supplementary Methods 5.

Construction of weighted gene co-expression and immune infiltration analysis

To elucidate genetic interactions and identify potential biomarkers or therapeutic targets for AECOPD with *P. aeruginosa* infection, we applied the Weighted correlation network analysis (WGCNA) framework using the "WGCNA" package in R software (version 4.3.2) [20]. Initial data preprocessing was performed to remove outliers, followed by the construction of a correlation matrix. An optimal soft-threshold power was then applied to convert this correlation matrix into an adjacency matrix, which was subsequently transformed into a topological overlap matrix (TOM). Gene modules were identified using average linkage hierarchical clustering based on TOM-based dissimilarity, and modules significantly associated with P. aeruginosa infection were selected for further analysis.

For immune cell infiltration analysis, the CIBERSORTx platform (https://cibersortx.stanford.edu/) was utilized. Its deconvolution algorithm quantified the abundance and proportions of 22 immune cell types from transcriptomic signatures in BALF and peripheral blood samples. This analysis included samples from both healthy individuals and patients with AECOPD with *P. aeruginosa* infection in the discovery cohort [21].

Proteomics statistical analysis

The proteomics data were statistically analyzed using Perseus software (version 1.6.15.0) [22] and R software

(version 4.3.2). This comprehensive analysis included hierarchical clustering at both the protein and peptide levels, with sequence annotation performed using databases such as UniProtKB/Swiss-Prot, Kyoto Encyclopedia of Genes and Genomes (KEGG), and Gene Ontology (GO). Enrichment analyses for GO terms and KEGG pathways were performed using Fisher's exact test, with multiple comparison controlled by false discovery rate (FDR) correction. GO terms were categorized into biological processes (BP), molecular functions (MF), and cellular components (CC), with pathways considered statistically significant at an adjusted p-value threshold of < 0.05. Additionally, PPI networks were constructed using the STRING database and visualized using Cytoscape software to elucidate the interactions among differentially expressed proteins (DEPs). The integration of our analyses was depicted through a Venn diagram, highlighting the convergence of hub genes identified via WGCNA and immune infiltration analysis, thereby prioritizing pivotal hub proteins for further investigation. For details, see Supplementary Methods 6.

Transcriptomics statistical analysis

Differential expression analysis between two groups was performed using the DESeq2 R package (version 1.18.1). DESeq2 employs statistical routines based on a negative binomial distribution model to determine differential expression in digital gene expression data. Resulting p-values were adjusted for multiple testing using the Benjamini-Hochberg method to control the false discovery rate. Transcriptomic analyses of GO and KEGG pathways, as well as immune infiltration, were conducted in parallel with proteomic analyses. Integration of proteomic and transcriptomic data was achieved using Venn diagrams to highlight the identification of BALF proteins and peripheral blood genes, thereby elucidating both local and systemic mechanisms of disease. For details, see Supplementary Methods 6.

Prediction of potential therapeutic agents and molecular Docking

To predict potential therapeutic agents for AECOPD with *P. aeruginosa* infection, the DSigDB database (http://tanlab.ucdenver.edu/DSigDB) was used to identify protein-drug interactions. Selection criteria included an FDR < 0.05 and a composite score > 5000. Three-dimensional (3D) structures of the compounds were obtained from the PubChem database in SDF format and converted to PDB format using Open Babel 2.3.2. Protein structures in PDB format were sourced from the Protein Data Bank (PDB). Water molecules and unrelated small molecule ligands were removed from these structures using PyMOL 2.5.1. The protein and ligand files were then converted to PDBQT format using AutoDockTools 1.5.6. Molecular docking simulations were performed using AutoDock Vina 1.1.2 within the Discovery Studio (version 2016) environment. Binding energies below -6 kcal/mol were considered indicative of strong affinity, signifying energetically favorable ligand-receptor interactions.

Statistical analysis

Statistical analysis of clinical data

Clinical data were analyzed using SPSS software (version 26.0). Continuous variables were analyzed with the Student's t-test, while categorical variables were assessed using Fisher's exact test. Results were presented as mean ± standard deviation (SD), with a p-value < 0.05 considered statistically significant. Correlation analyses were performed using R software (version 4.3.2) to explore associations between clinical parameters in detail.

Receiver operating characteristic (ROC) curve validation

The diagnostic efficacy of identified hub genes was evaluated using ROC curve analysis with the "pROC" package in R software (version 4.3.2). This analysis calculated the area under the curve (AUC) and provided a 95% confidence interval (CI). Biomarkers with an AUC exceeding 0.7 was deemed diagnostically relevant, demonstrating a strong capability to discriminate between disease states [23].

Visualization and target identification methods

The "EnhancedVolcano" package was used for volcano plots, displaying the significance and magnitude of protein expression changes. "clusterProfiler" facilitated GO/KEGG enrichment analysis, while "pheatmap" generated heatmaps of protein expression patterns. "WGCNA" was applied to visualize co-expression networks, and "VennDiagram" showed overlaps between datasets. We used "circlize" for chord diagrams to illustrate relationships between gene sets and pathways, and ggplot2 for box plots and lollipop plots to compare protein expression levels and highlight key biomarkers. "corrplot" was used to create correlation heatmaps. Additionally, Cytoscape was used for target identification, with MCC prioritizing central proteins in the network and MCODE identifying densely connected protein complexes. For details, see Supplementary Methods 6.

Results

Clinical biomarker analysis in AECOPD with *P. aeruginosa* infection

The basic clinical characteristics and inflammatory markers of the discovery cohort (Table 1), which includes 40 AECOPD with *P. aeruginosa* infection patients and 20 healthy controls, are summarized. The COPD P.A.

Table 1 Basic information of discovery cohort

Characteristics	COPD *P.A.* group	Control group	*P*
No.	40	20	
Age, year	66.16 ± 7.59	63.10 ± 10.26	0.195
BMI, kg/m^2	22.67 ± 2.25	23.67 ± 1.73	0.086
Smoking			
Current smoker	92.5% (37)	60% (12)	0.02
Pack-years	39 (23.38, 50.00)	17.50 (0.00, 30.00)	0.004
Lung Function			
FEV1, L	1.34 ± 0.56	2.83 ± 0.69	< 0.001
FVC, L	2.98 ± 0.74	3.59 ± 0.87	0.007
FEV1/FVC	0.44 ± 0.12	0.79 ± 0.05	< 0.001
GOLD-stage			
I	10% (4)	/	/
II	37.5% (15)	/	/
III	45% (18)	/	/
IV	7.5% (3)	/	/
Inflammatory markers			
WBC,10^9/L	9.81 ± 1.30	6.59 ± 1.63	< 0.001
NEU,10^9/L	7.43 ± 0.82	3.55 ± 0.91	< 0.001
LYM,10^9/L	1.50 ± 0.56	2.39 ± 0.83	< 0.001
MONO,10^9/L	0.47 ± 0.18	0.49 ± 0.18	0.729
EOS,10^9/L	0.23 ± 0.20	0.16 ± 0.08	0.081

FEV1: Forced expiratory volume in one second; **FVC**: Forced vital capacity; **WBC**: White blood cell; **NEU**: Neutrophil; **LYM**: Lymphocyte; **MONO**: Monocyte; **EOS**: Eosinophil

Table 2 Basic information of validation cohort

Characteristics	COPD *P.A.* group	Control group	*P*
No.	20	10	
Age, year	67.15 ± 8.99	63.7 ± 5.69	0.280
BMI, kg/m^2	22.39 ± 3.33	24.04 ± 1.44	0.147
Smoking			
Current smoker	100% (20)	50% (5)	< 0.001
Pack-years	32.50 (25.00, 50.00)	15 (0.00, 36.25)	0.039
Lung Function			
FEV1, L	1.48 ± 0.44	2.64 ± 0.75	< 0.001
FVC, L	3.03 ± 0.63	3.52 ± 1.14	0.233
FEV1/FVC	0.49 ± 0.09	0.76 ± 0.05	< 0.001
GOLD-stage			
I	5% (1)	/	/
II	65% (13)	/	/
III	30% (6)	/	/
IV	0% (0)	/	/
Inflammatory markers			
WBC,10^9/L	9.84 ± 0.93	6.29 ± 0.99	< 0.001
NEU,10^9/L	7.12 ± 1.12	3.20 ± 0.66	< 0.001
LYM,10^9/L	1.79 ± 0.51	2.27 ± 0.43	0.015
MONO,10^9/L	0.49 ± 0.09	0.41 ± 0.15	0.074
EOS,10^9/L	0.28 ± 0.22	0.19 ± 0.06	0.204

FEV1: Forced expiratory volume in one second; **FVC**: Forced vital capacity; **WBC**: White blood cell; **NEU**: Neutrophil; **LYM**: Lymphocyte; **MONO**: Monocyte; **EOS**: Eosinophil

group had a mean age of 66.16 ± 7.59 years, compared to 63.10 ± 10.26 years in the control group ($P = 0.195$). The COPD P.A. group exhibited significantly reduced lung function with FEV1 values of 1.34 ± 0.56 L versus 2.83 ± 0.69 L ($P < 0.001$), FVC values of 2.98 ± 0.74 L versus 3.59 ± 0.87 L ($P = 0.007$), and an FEV1/FVC ratio of 0.44 ± 0.12 compared to 0.79 ± 0.05 ($P < 0.001$). Inflammatory markers were also significantly higher in the COPD P.A. group, with WBC levels reaching $9.81 \pm 1.30 \times 10^9$/L compared to $6.59 \pm 1.63 \times 10^9$/L in the control group ($P < 0.001$), and NEU at $7.43 \pm 0.82 \times 10^9$/L versus $3.55 \pm 0.91 \times 10^9$/L ($P < 0.001$).

The validation cohort (Table 2) included 20 AECOPD with *P. aeruginosa* infection patients and 10 healthy controls. The COPD P.A. group had a mean age of 67.15 ± 8.99 years compared to 63.7 ± 5.69 years in the control group ($P = 0.280$). The COPD P.A. group demonstrated significantly reduced lung function, with FEV1 values of 1.48 ± 0.44 L versus 2.64 ± 0.75 L ($P < 0.001$), and an FEV1/FVC ratio of 0.49 ± 0.09 compared to 0.76 ± 0.05 ($P < 0.001$). Inflammatory markers were higher in the COPD P.A. group, with WBC levels reaching $9.84 \pm 0.93 \times 10^9$/L compared to $6.29 \pm 0.99 \times 10^9$/L in the control group ($P < 0.001$), and NEU at of $7.12 \pm 1.12 \times 10^9$/L compared to $3.20 \pm 0.66 \times 10^9$/L ($P < 0.001$).

The number of current smokers and number of smoking packs a year were significantly higher in the COPD group than in the healthy control group($P < 0.05$). Moreover, the basic clinical features and inflammatory markers of COPD and control groups did not differ significantly between the discovery cohort and the validation cohort (Table S1 and S2).

Proteomic insights from BALF identify biomarker candidates

We detected a total of 592 valid proteins (Dataset 1). In our exploration of the proteomic landscape within BALF from a discovery cohort comprising 40 AECOPD with *P. aeruginosa* infection patients and 20 healthy controls, we utilized the 'limma' package in R to identify 100 differentially expressed proteins (DEPs). Of these, 77 were up-regulated and 23 down-regulated, adhering to our predefined selection criteria of an absolute log2 fold change greater than 1.5 and an adjusted *p*-value less than 0.05 (Dataset 2). The proteomic signatures distinguishing AECOPD with *P. aeruginosa* infection patients from healthy controls were visualized through volcano plots (Fig. 2A).

GO enrichment analysis of these differentially expressed proteins provides deeper insights into the affected biological processes, cellular components, and molecular functions (Dataset 3). Enriched biological processes (Fig. 2B) include "defense response to bacteria,"

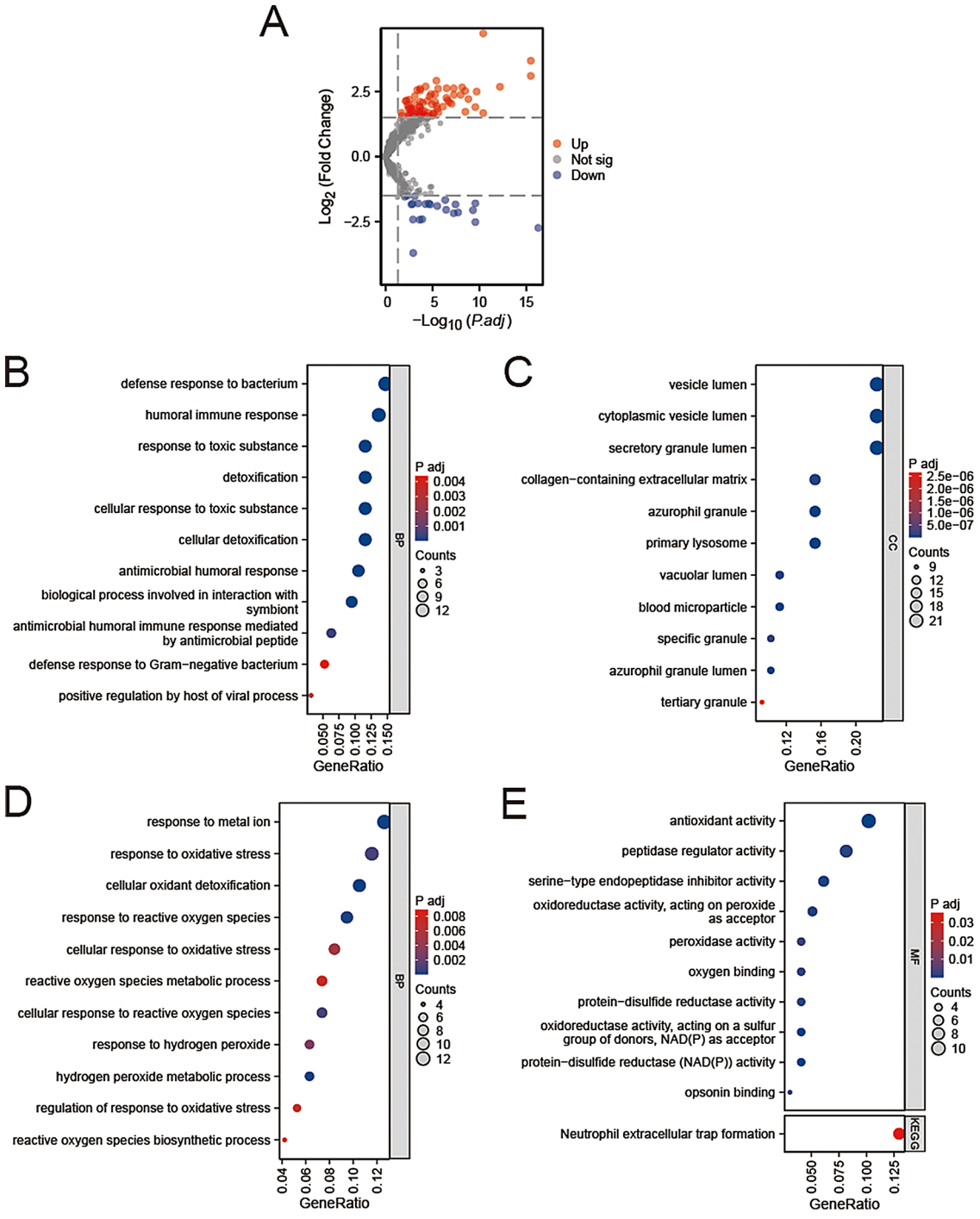

Fig. 2 Differential Protein Expression and Functional Insights in BALF of AECOPD with *P. aeruginosa* infection. **(A)** Volcano plots highlight differentially expressed proteins (DEPs) within the cohort, identifying key proteins of interest based on statistical and biological significance. **(B-E)** Functional categorization and pathway enrichment analyses of the 100 identified DEPs, utilizing Gene Ontology (GO) and Kyoto Encyclopedia of Genes and Genomes (KEGG), underscore critical biological processes and pathways. These include defense response to bacteria, humoral immune response, oxidative stress, metal ion handling, and antioxidant activity within the GO framework, and neutrophil extracellular trap formation within KEGG pathways

"humoral immune response," and "response to toxic substance". Enriched cellular components (Fig. 2C), such as "vesicle lumen," "cytoplasmic vesicle lumen," and "collagen-containing extracellular matrix," indicate substantial alterations in intracellular vesicular transport and extracellular matrix composition. The pathway analysis (Fig. 2D) reveals significantly enriched pathways such as "response to metal ion," "response to oxidative

stress," and "cellular response to reactive oxygen species". Enriched molecular functions (Fig. 2E) include "antioxidant activity," "peptidase regulator activity," and "oxidoreductase activity," which are essential for mitigating oxidative damage and maintaining protein homeostasis. KEGG pathway enrichment further linked these differentially expressed proteins to neutrophil extracellular trap formation (Fig. 2E).

WGCNA in AECOPD with *P. aeruginosa* infection

Protein clustering and WGCNA revealed five distinct modules of co-expressed key proteins of 592 valid proteins (Supplementary Figures S1). The yellow module comprised 11 proteins, the blue module contained 18 proteins, the brown module included 13 proteins, and the gray module consisted of 2 proteins, totaling 44 proteins across all WGCNA modules (Fig. 3A, Dataset 4). Correlating these modules with specific sample traits elucidated the complex biological interactions underlying the disease, offering a deeper insight into its molecular intricacies (Fig. 3B).

Subsequent GO and KEGG pathway analyses, particularly of the yellow module, highlighted the critical roles of acute inflammatory responses and pathways involved in coagulation, blood microparticle, complement and coagulation cascades and ferroptosis (Fig. 3C, Dataset 5), which are central to the host acute phase response. The analysis of the blue module revealed the host defense strategies, emphasizing superoxide metabolic process, neutrophil mediated immunity, neutrophil degranulation, reactive oxygen species metabolic process, sulfur compound binding and antioxidant activities (Fig. 3D, Dataset 6). Notably, key pathways such as neutrophil extracellular trap formation and the Leukocyte transendothelial migration pathway were highlighted in the blue module, shedding light on essential immune response mechanisms. The brown module's exploration (Fig. 3E, Dataset 7) illuminated processes essential for maintaining structural and functional integrity under infection, including regulation of endopeptidase activity, sequestering of metal ion, intrinsic apoptotic signaling pathway and cellular response to reactive oxygen species, indicating the body's effort to preserve homeostasis. The grey module's analysis (Fig. 3F, Dataset 8) further underscored these adaptive mechanisms by highlighting critical pathways involved in cell mediated cytotoxicity.

Integrative analysis of differentially expressed proteins and Co-expression modules in AECOPD with *P. aeruginosa* infection

In our integrative analysis of 100 DEPs and 44 WGCNA proteins, we identified significant overlap and distinct features of AECOPD with *P. aeruginosa* infection. The Venn diagram (Fig. 4A, Dataset 9) shows 18 AECOPD with *P. aeruginosa* infection differentially expressed proteins (PACDEPs), highlighting the robustness and relevance of our findings. A heatmap (Fig. 4B) illustrates the expression patterns of PACDEPs across control and COPD P.A. groups, revealing clear distinctions in protein expression. Boxplots (Fig. 4C) further quantify the expression levels of PACDEPs, including ITIH4, PLS3, MNDA, LCN2, AZU1, MPO, and others, confirming their significant differential expression between the two groups.

Functional enrichment analyses provide deeper insights into the biological roles of PACDEPs (Dataset 10). GO and KEGG analysis (Fig. 4D) shows significant enrichment in processes such as negative regulation of peptidase activity, response to reactive oxygen species, and neutrophil-mediated killing of bacteria. The cellular component analysis indicates enrichment in vesicle lumens, cytoplasmic vesicle lumens, and azurophil granules, suggesting alterations in intracellular transport and immune responses. Molecular function analysis highlights enzyme inhibitor activity, peptidase regulator activity, and antioxidant activity, underscoring the importance of protease regulation and oxidative stress management in the disease. Circular plots (Fig. 4E) provide a comprehensive view of the interactions between these proteins and their associated GO and KEGG terms. AZU1, MPO, RETN and other proteins were found to be important in multiple pathways. The emphasis on oxidative stress pathways and neutrophil extracellular traps is consistent with clinical observations of elevated neutrophil levels.

Immune cell profiling and correlation with differentially expressed proteins in BALF of AECOPD with *P. aeruginosa* infection

To explore the immune landscape in BALF of AECOPD with *P. aeruginosa* infection, we performed an in-depth analysis of immune cell populations and their correlation with DEPs. Bar plots (Fig. 5A, Dataset 11) quantified the relative expression levels of various immune cell types, showing significant differences in cell populations, particularly in macrophages, neutrophils, and T cells, between the two groups.

The correlation heatmap (Fig. 5B) illustrated the relationships between various immune cell types, revealing significant correlations that provide insights into the immune network alterations in AECOPD with *P. aeruginosa* infection. Notably, there is a strong positive correlation between NK cells and macrophages (both M1 and M2 types), a positive correlation between neutrophils and T-cells, but a negative correlation between neutrophils and macrophages (both M1 and M2 types). These interactions suggest a coordinated response between NK cells and macrophages, neutrophils and T-cells to fight the bacterial infection. The correlations between T

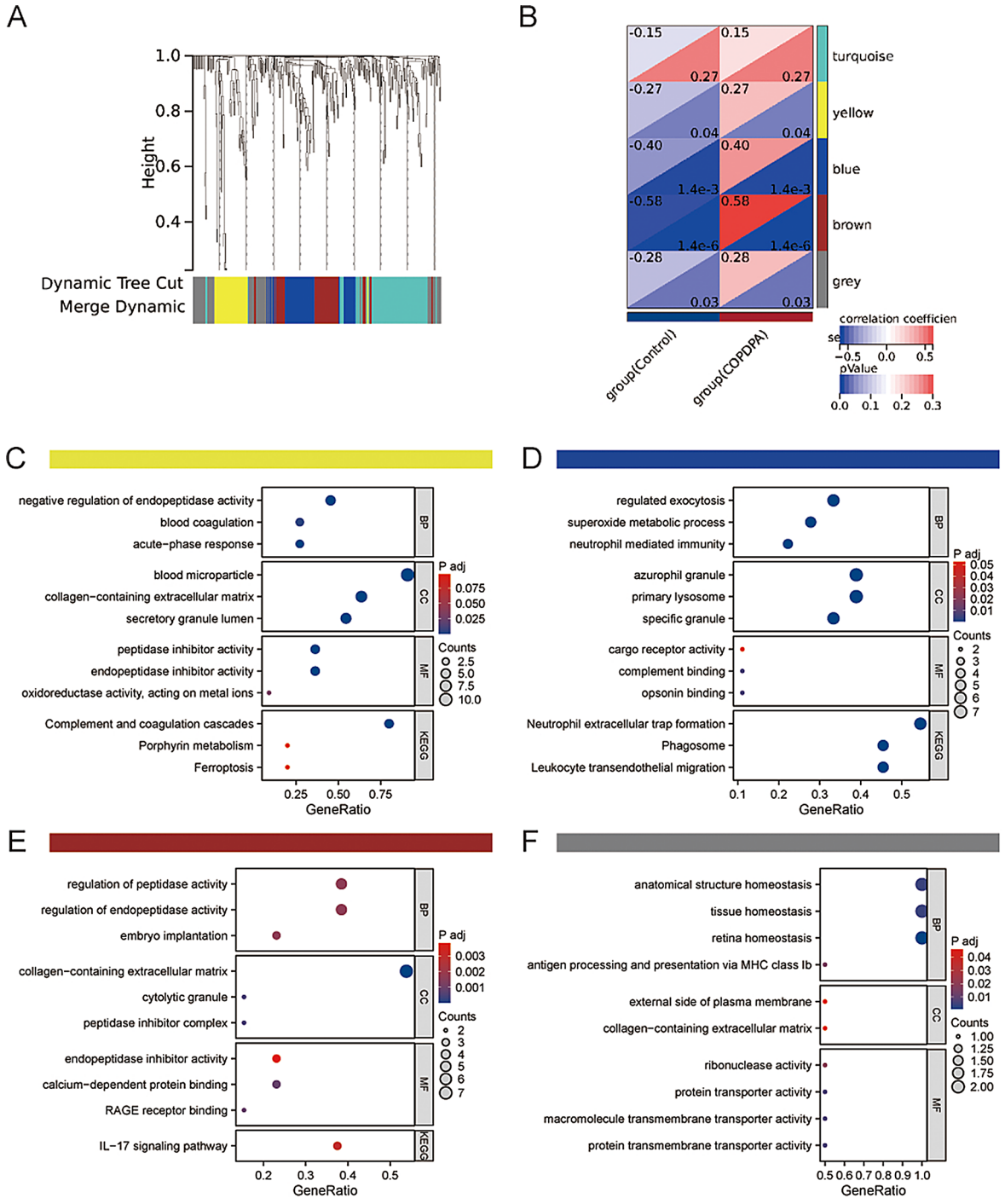

Fig. 3 Weighted Gene Co-expression Network Analysis (WGCNA) in AECOPD with *P. aeruginosa* Infection. **(A)** Cluster dendrogram displaying modules of co-expressed proteins, identified by dynamic tree cut. **(B)** Heatmap showing the correlation between module eigengenes and sample traits, with correlation coefficients and *p*-values. **(C)** GO and KEGG pathway enrichment analyses for the yellow module, highlighted the critical roles of acute inflammatory responses. **(D)** Neutrophil extracellular trap formation and the Leukocyte transendothelial migration pathway were highlighted in the blue module. **(E)** The brown module's exploration illuminated processes essential for maintaining structural and functional integrity under infection. **(F)** Analyses for the grey module, indicating cell mediated cytotoxicity

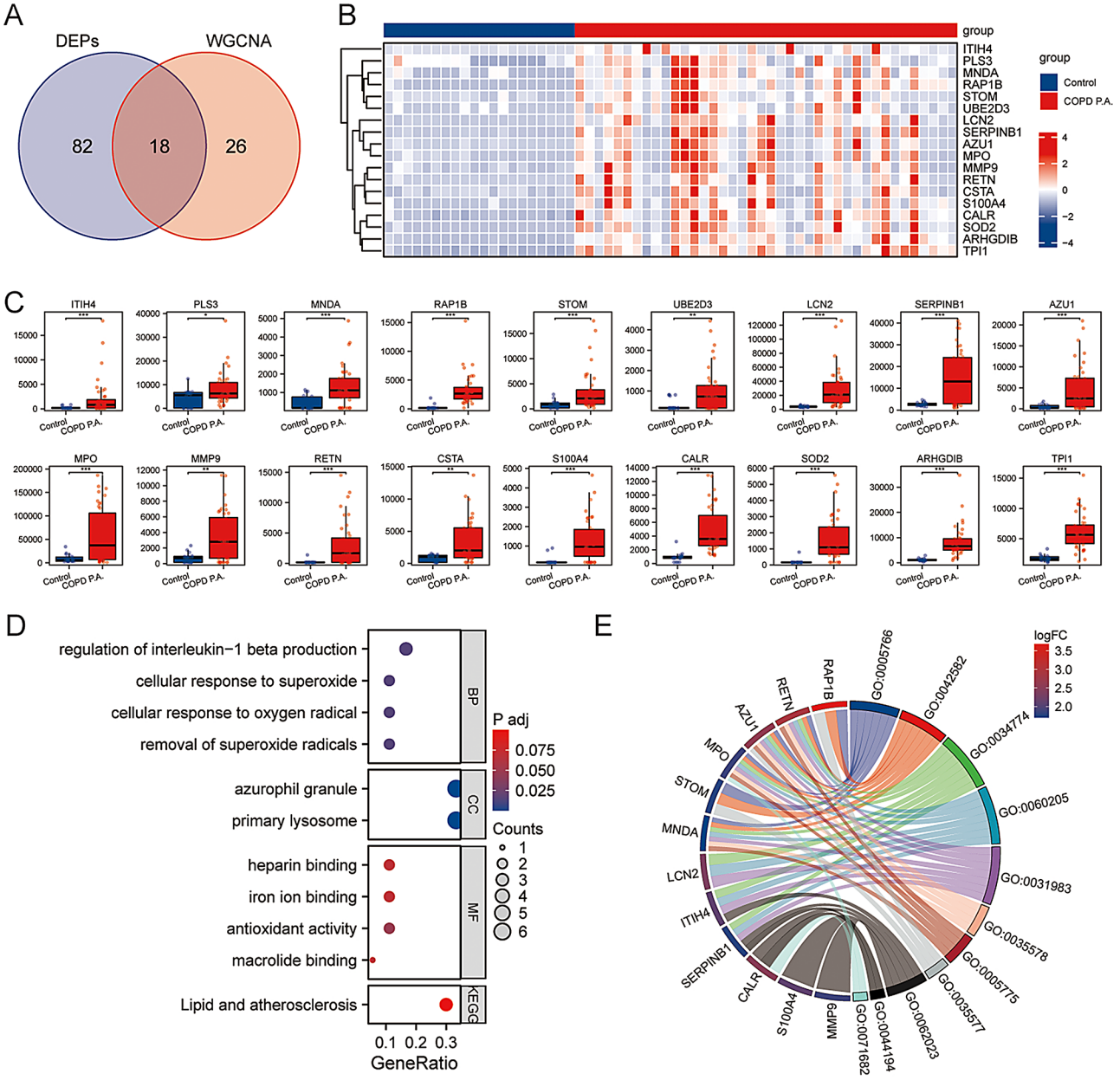

Fig. 4 Integrative Analysis of Differentially Expressed Proteins and Co-expression Modules in AECOPD with *P. aeruginosa* infection. **(A)** Venn diagram showing the overlap between differentially expressed proteins (DEPs) and WGCNA modules. **(B)** Heatmap illustrating expression patterns of common proteins across control and COPD P.A. groups. **(C)** Boxplots of selected DEPs, confirming significant differential expression. **(D)** Gene Ontology (GO) and Kyoto Encyclopedia of Genes and Genomes (KEGG) enrichment analyses: Biological processes, Cellular components, and Molecular functions and Kyoto Encyclopedia of Genes and Genomes. **(E)** Circular plots mapping protein interactions and associated GO terms. *, $P < 0.05$. **, $P < 0.01$.***, $P < 0.001$

cell subsets, such as CD8 + T cells and regulatory T cells (Tregs), highlighting the role of complex immune regulatory mechanisms.

Detailed correlation analyses (Supplementary Figures S2) between specific DEPs and immune cell types further elucidated the immune response dynamics. For instance, AZU1, MPO, MMP9, and RETN showed significant positive correlations with activated NK cells and M1 macrophages, suggesting their roles in enhancing the immune response against P. aeruginosa. Conversely, proteins such as RAP1B and STOM were more closely associated with neutrophils and T cell subsets, indicating their involvement in modulating specific aspects of the immune response. The expression of MPO, a marker for neutrophils, was significantly elevated in the COPD P.A. group, aligning with the increased neutrophil levels observed in these patients. Similarly, elevated levels of CSTA and

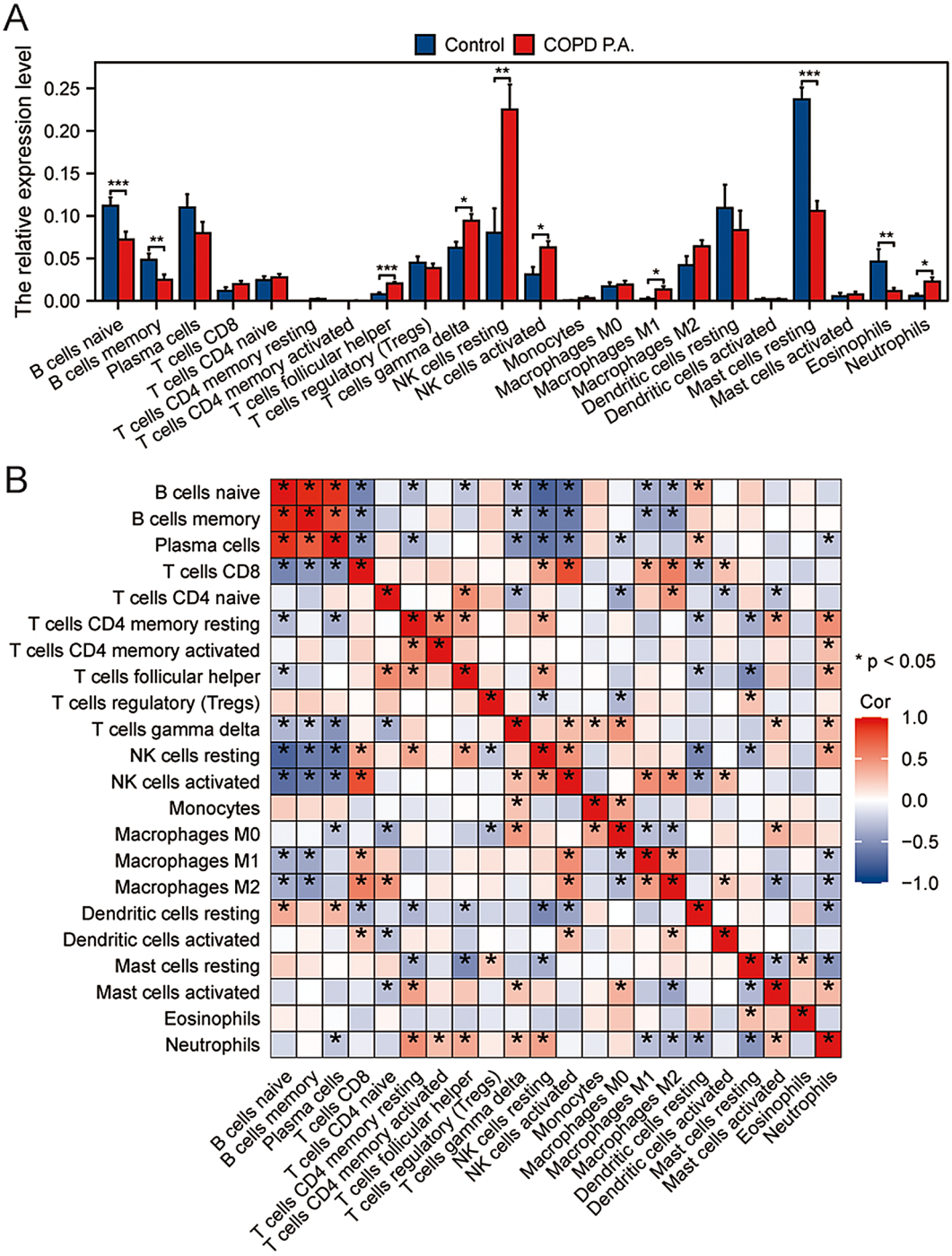

Fig. 5 Immune Cell Profiling and Correlation with Differentially Expressed Proteins in BALF of AECOPD with *P. aeruginosa* infection. **(A)** Bar plots quantifying the relative expression levels of various immune cell types, highlighting significant differences in cell populations. **(B)** Correlation heatmap illustrating relationships between different immune cell types, revealing significant correlations and network alterations. *, $P < 0.05$. **, $P < 0.01$.***, $P < 0.001$

S100A4 in macrophages further highlight the activation state of these cells in response to bacterial infection.

Circulating biomarkers and immune landscape in AECOPD with *P. aeruginosa* infection

We detected 592 valid proteins in the plasma proteomics dataset (Dataset 12). To further elucidate the molecular landscape of AECOPD with *P. aeruginosa* infection, plasma proteomics analysis identified 25 upregulated and 15 downregulated proteins in the COPD P.A. group compared to controls, based on our predefined criteria of an absolute log2 fold change greater than 1 and an adjusted p-value less than 0.05 (Fig. 6A, Dataset 13). GO and KEGG enrichment analyses of these differentially expressed proteins revealed key pathways (Fig. 6B, Dataset14), including inflammatory responses and neutrophil-mediated immunity. Cellular component analysis highlighted the enrichment of azurophil granules and lysosomes, both essential for neutrophil activity, while molecular function analysis showed significant enrichment in serine-type endopeptidase activity, further supported by KEGG's identification of neutrophil extracellular trap formation as a critical pathway, which exacerbates tissue damage.

We detected 20,504 valid RNAs in the peripheral blood transcriptomic dataset (Dataset 15). Transcriptomic analysis of peripheral blood identified 821 upregulated and 422 downregulated genes, based on our selection criteria of an absolute log2 fold change greater than 1.5 and an adjusted p-value less than 0.05 (Fig. 6C, Dataset 16). Functional enrichment analysis of these differentially expressed genes revealed significant biological processes, particularly those related to leukocyte migration, regulation of inflammatory responses, and defense against bacterial molecules (Fig. 6D, Dataset 17). Additionally, pathways related to granulocyte and neutrophil migration, chemotaxis, and macrophage activation were notably enriched, suggesting that these immune cells are not only more numerous but also more active in the disease state. Cellular component analysis revealed significant involvement of vesicle lumens, cytoplasmic vesicle lumens, and specific granules, all of which are critical to immune cell function and pathogen response, further contributing to tissue damage. Immune infiltration analysis demonstrated a significant increase in neutrophils and macrophages in the COPD P.A. group (Fig. 6E, Dataset 18). The correlation matrix further elucidated the relationships between various immune cell types, revealing a complex network of interactions that are significantly altered in AECOPD with *P. aeruginosa* infection patients. There was a significant positive correlation between neutrophils, T cells gamma delta, and monocytes, indicating a coordinated immune response to bacterial infection (Fig. 6F).

Integration of plasma proteomics and peripheral blood transcriptomics identified six overlapping biomarkers (Fig. 6G, Dataset 19): C1QA, AZU1, ELANE, RETN, MPO, CTSG. GO and KEGG enrichment analyses of these biomarkers showed significant associations with antimicrobial responses and neutrophil-mediated bacterial killing, with NET formation being notably enriched, emphasizing its damaging role in AECOPD with *P. aeruginosa* infection (Fig. 6H-I, Dataset 20).

Integration of BALF proteomics and plasma proteomics in AECOPD with *P. aeruginosa* infection

To identify key molecular targets in AECOPD with *P. aeruginosa* infection, we integrated DEPs from BALF proteomics with DEPs from plasma proteomics. The Venn diagram (Fig. 7A, Dataset 21) shows the overlap between the DEPs, revealing 7 common targets. Protein-protein interaction network analysis using STRING (Fig. 7B) was performed on these 7 common targets, highlighting a highly interconnected network. Common targets such as AZU1, MPO, RETN, and CTSG emerged as central nodes, suggesting their pivotal roles in the pathophysiology of AECOPD with *P. aeruginosa* infection.

Functional enrichment analyses provided insights into the biological processes, cellular components, molecular functions, and pathways associated with these common targets (Dataset 22). GO analysis (Fig. 7C) revealed significant enrichment in processes such as defense response to bacteria, humoral immune response, neutrophil-mediated killing of bacterium and defense response to Gram-negative bacterium. Additionally, there was a substantial enrichment of pathways related to oxidative stress (Fig. 7D). These processes were critical for the host defense against bacterial infections and underline the heightened immune activity in COPD P.A. patients. Cellular component analysis (Fig. 7F) identified significant enrichment in vesicle lumen, cytoplasmic vesicle lumen, and specific granules, highlighting the involvement of these components in immune cell functions and antimicrobial activities. Molecular function analysis (Fig. 7G) revealed enrichment in activities such as glycosaminoglycan binding, endopeptidase activity, peroxidase activity and serine-type peptidase activity, indicating the roles of these proteins in extracellular matrix degradation and immune modulation.

KEGG pathway analysis emphasized the critical involvement of neutrophil-related pathways, including Neutrophil extracellular trap formation. The enrichment of pathways related to neutrophil activation and function aligns with clinical observations of increased neutrophil levels and activity in COPD P.A. group patients, highlighting their contribution to disease pathology and potential as therapeutic targets.

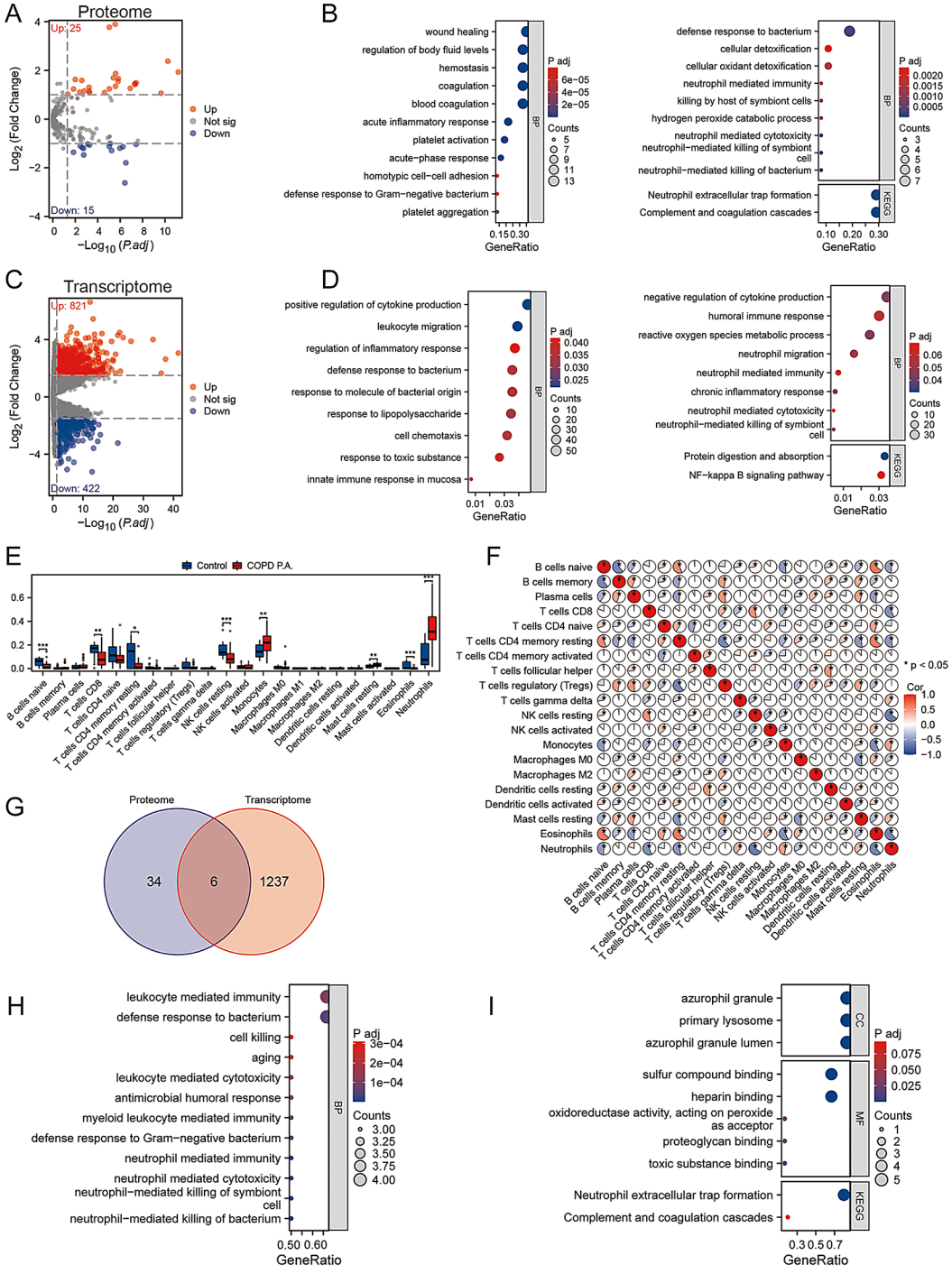

Fig. 6 Plasma proteomics and peripheral blood transcriptomics analyses in AECOPD with *P. aeruginosa* infection. **(A)** Plasma proteomics identified 25 upregulated and 15 downregulated proteins. **(B)** GO analysis showed enrichment in inflammatory responses and neutrophil-mediated immunity. Azurophil granules and lysosomes were enriched in cellular component analysis. Molecular function and KEGG analysis highlighted serine-type endopeptidase activity and NET formation. **(C)** Transcriptomics identified 821 upregulated and 422 downregulated genes. **(D)** Enrichment analyses indicated pathways related to leukocyte migration, neutrophil chemotaxis, and macrophage activation. **(E)** Immune infiltration analysis revealed increases in neutrophils and macrophages. **(F)** The correlation matrix showed interactions between immune cell types. **(G)** Six overlapping biomarkers were identified. **(H-I)** GO and KEGG analysis highlighted antimicrobial responses and NET formation. *, $P < 0.05$. **, $P < 0.01$.***, $P < 0.001$

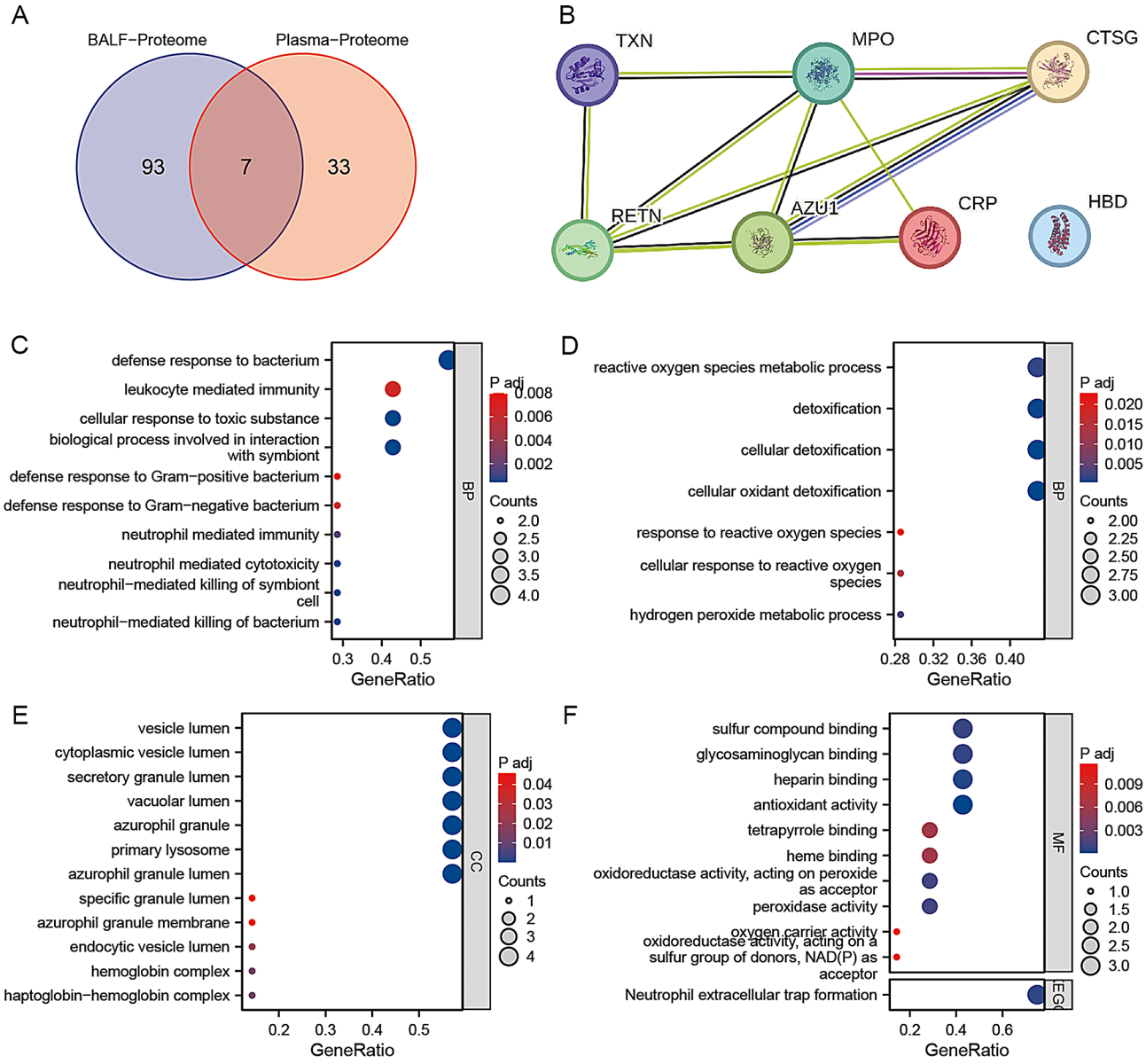

Fig. 7 Integration of BALF Proteomics and Plasma Proteomics in AECOPD with *P. aeruginosa* Infection. **(A)** Venn diagram showing the overlap between DEPs from BALF proteomics and DEPs from plasma proteomics, identifying 7 common targets. **(B)** STRING network analysis of the 15 common targets, illustrating their interactions and highlighting key proteins. **(C-F)** Functional enrichment analyses: **(C, D)** Biological processes highlighting immune responses, neutrophil-mediated killing of bacterium, defense response to Gram-negative bacterium and oxidative stress pathways **(E)** Cellular components involved in immune functions and antimicrobial activities, and **(F)** Molecular functions indicating roles in extracellular matrix degradation and immune modulation. KEGG pathway analysis further emphasizes neutrophil-related pathways, including neutrophil extracellular trap formation, crucial for understanding the immune response in AECOPD with P. aeruginosa infection

Validation and functional analysis of key proteins in BALF proteomics of AECOPD with *P. aeruginosa* infection

We conducted an in-depth proteomic analysis of BALF from AECOPD with *P. aeruginosa* infection patients, focusing on DEPs. Using STRING for PPI network analysis, we identified interacting proteins. This network was further analyzed using Cytoscape to perform MCC and MCODE analyses, identifying highly interconnected clusters of proteins (Fig. 8A, B). By intersecting these clusters with BALF-proteome, plasma-proteome and proteins of WGCNA, we identified three key proteins: AZU1, MPO, and RETN (Fig. 8C, Dataset 23). Functional enrichment analyses of these proteins highlighted significant GO terms related to defense responses to bacteria, aging, oxidative stress, and neutrophil activity (Fig. 8D, Dataset 24). KEGG pathway analysis revealed enrichment in pathways involving NETs formation (Fig. 8E).

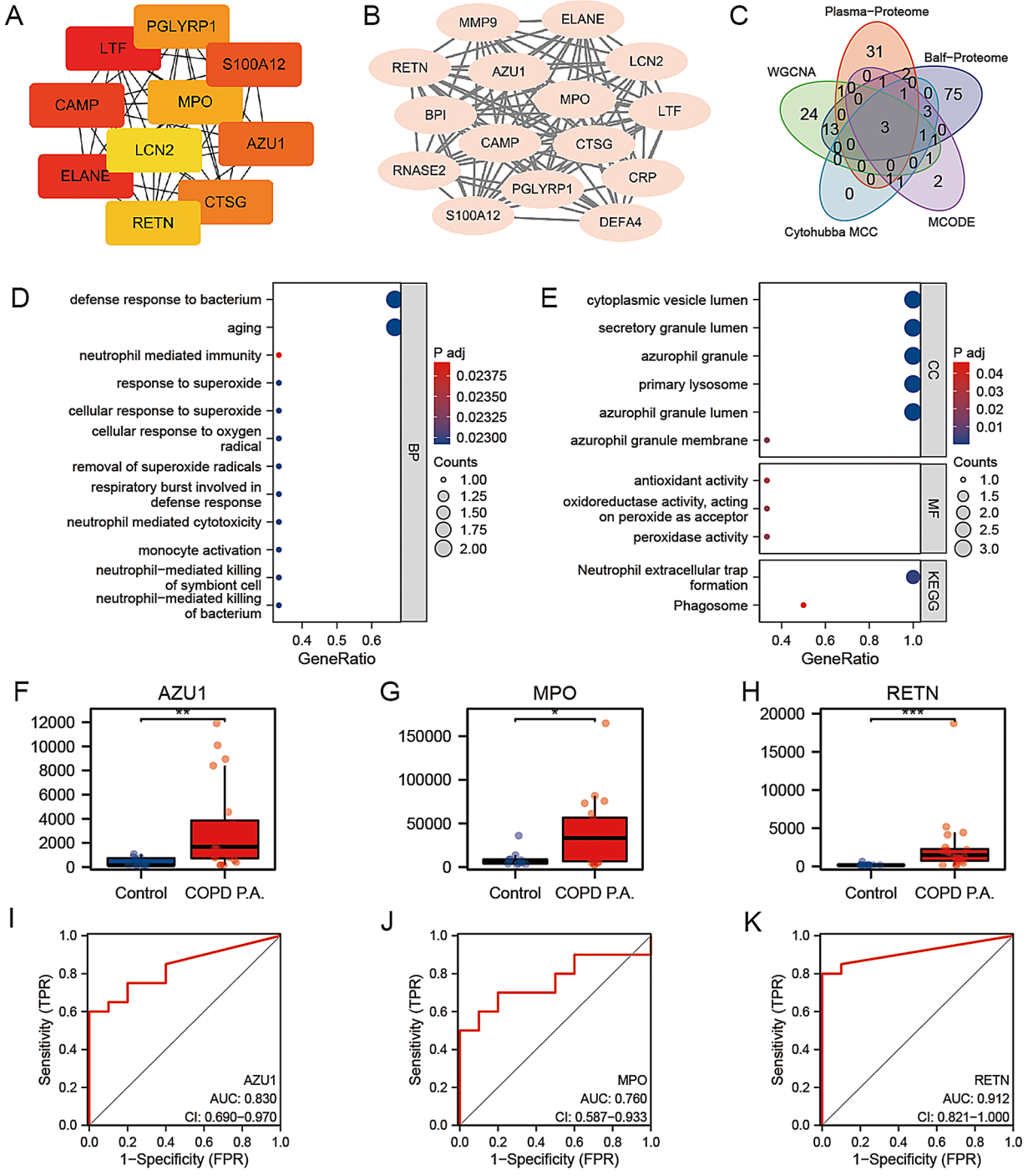

Fig. 8 Validation and Functional Analysis of Key Proteins of AECOPD with *P. aeruginosa* Infection. **(A)** MCC analysis using Cytoscape, identifying key protein clusters. **(B)** MCODE analysis highlighting densely interconnected proteins. **(C)** Venn diagram showing intersection of MCC, MCODE, Balf-proteome, Plasma-proteome and WGCNA analyses, identifying three key proteins. **(D)** GO enrichment analysis of the three key proteins, highlighting immune response and oxidative stress-related processes. **(E)** KEGG pathway analysis showing enrichment in vesicle lumen an NET formation pathway. (**F-K**0 Box plots and ROC curves for AZU1, MPO, and RETN, confirming their differential expression and diagnostic value. *, $P < 0.05$. **, $P < 0.01$.***, $P < 0.001$

For validation, we analyzed an independent cohort of 20 AECOPD with *P. aeruginosa* infection patients and 10 controls (Dataset 25). Box plots confirmed the differential expression of these proteins in the validation cohort, with significant upregulation in the COPD P.A. group (Fig. 8F-H, Dataset 26). The diagnostic value of these proteins was assessed using ROC curves (Fig. 8I-K), which demonstrated high AUC values for each protein:

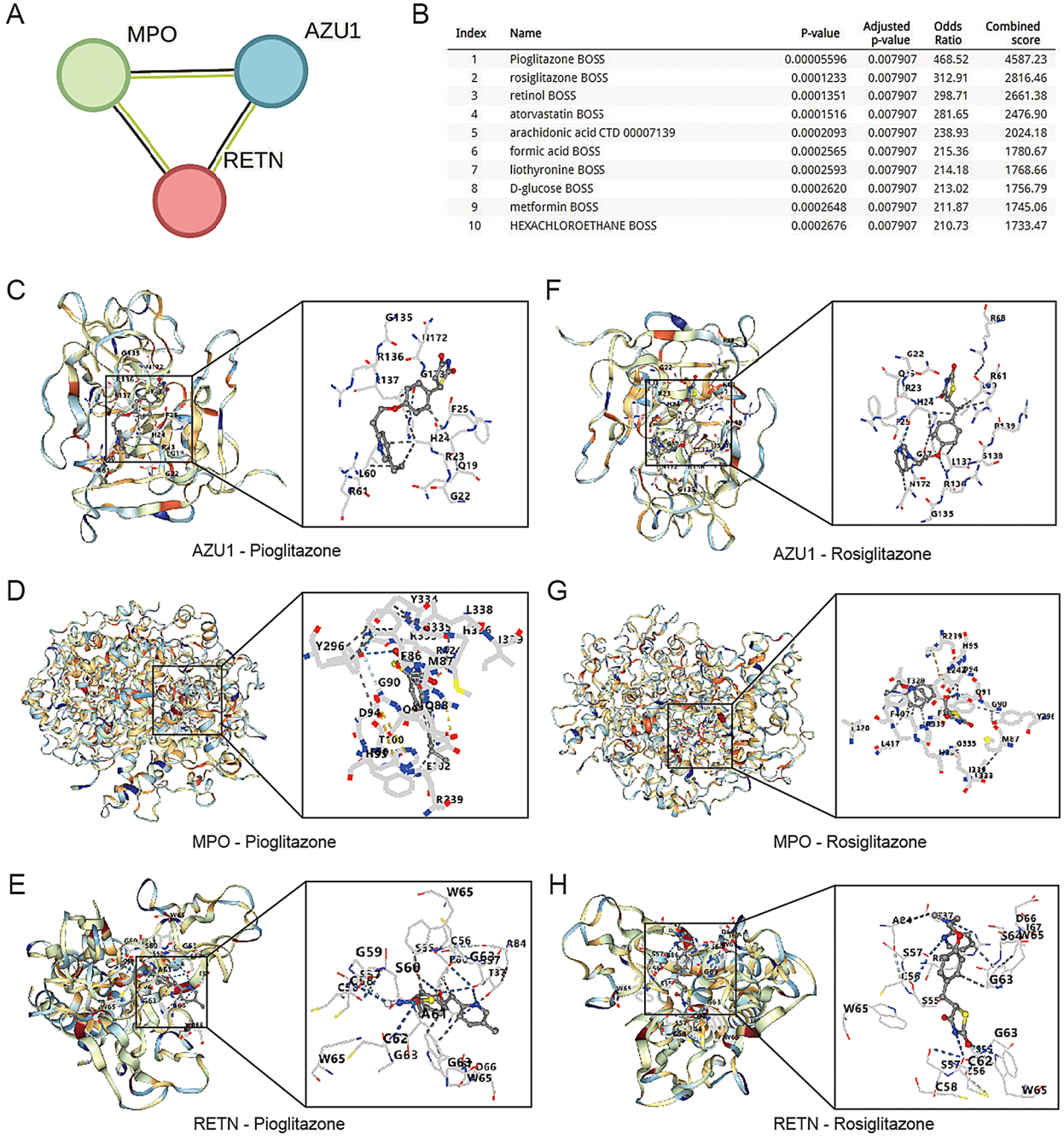

Index	Name	P-value	Adjusted p-value	Odds Ratio	Combined score
1	Pioglitazone BOSS	0.00005596	0.007907	468.52	4587.23
2	rosiglitazone BOSS	0.0001233	0.007907	312.91	2816.46
3	retinol BOSS	0.0001351	0.007907	298.71	2661.38
4	atorvastatin BOSS	0.0001516	0.007907	281.65	2476.90
5	arachidonic acid CTD 00007139	0.0002093	0.007907	238.93	2024.18
6	formic acid BOSS	0.0002565	0.007907	215.36	1780.67
7	liothyronine BOSS	0.0002593	0.007907	214.18	1768.66
8	D-glucose BOSS	0.0002620	0.007907	213.02	1756.79
9	metformin BOSS	0.0002648	0.007907	211.87	1745.06
10	HEXACHLOROETHANE BOSS	0.0002676	0.007907	210.73	1733.47

Fig. 9 Molecular Docking and Drug Screening for 3 Key Proteins. **(A)** Interaction network of the three key proteins (AZU1, MPO, and RETN). **(B)** Top 10 candidate molecules identified from the DSigDB database for potential therapeutic interaction with the key proteins, with Pioglitazone and Rosiglitazone highlighted. **(C-E)** Molecular docking simulations showing the binding of Pioglitazone to AZU1 (**(C)**) with a binding energy of -8.1 kcal/mol, MPO **(D)** with a binding energy of -9.2 kcal/mol, and RETN **(E)** with a binding energy of -8.1 kcal/mol. **(F-H)** Molecular docking simulations showing the binding of Rosiglitazone to AZU1 **(F)** with a binding energy of -7.4 kcal/mol, MPO **(G)** with a binding energy of -8.7 kcal/mol, and RETN **(H)** with a binding energy of -7.7 kcal/mol

AZU1 (AUC = 0.830), MPO (AUC = 0.760), and RETN (AUC = 0.912). These results suggested these proteins as robust biomarkers for distinguishing AECOPD with *P. aeruginosa* infection patients from healthy controls.

Molecular Docking and drug screening for key proteins in AECOPD with *P. aeruginosa* infection

To predict potential therapeutic agents for AECOPD with *P. aeruginosa* infection, we constructed an interaction network for the three key proteins (AZU1, MPO, and RETN) identified in our previous analyses (Fig. 9A).

Using the DSigDB database, we screened for small molecules that could interact with these proteins, resulting in the identification of the top 10 candidate molecules (Fig. 9B, Dataset 27). A review of the literature identified Pioglitazone and Rosiglitazone as having potential therapeutic value for lung diseases, and they were also the top two candidates in our screen.

Molecular docking simulations were performed to evaluate the binding affinities of Pioglitazone and Rosiglitazone with each of the three key proteins. The 3D structures of Pioglitazone and Rosiglitazone were obtained from the PubChem database and converted to PDB format using Open Babel 2.3.2. Protein structures in PDB format were sourced from the Protein Data Bank. Using PyMOL 2.5.1, water molecules and unrelated small molecule ligands were removed from these structures. The protein and ligand files were then converted to PDBQT format using AutoDockTools 1.5.6. Docking simulations were performed using AutoDock Vina 1.1.2 within the Discovery Studio (version 2016) environment. Binding energies below − 6 kcal/mol were considered indicative of strong affinity, signifying energetically favorable ligand-receptor interactions.

The docking results demonstrated strong binding affinities for Pioglitazone with the three key proteins. The binding energy for AZU1 was − 8.1 kcal/mol (Fig. 9C), for MPO was − 9.2 kcal/mol (Fig. 9D), and for RETN was − 8.1 kcal/mol (Fig. 9E). Similarly, Rosiglitazone also showed strong binding affinities, with binding energies of -7.4 kcal/mol for AZU1 (Fig. 9F), -8.7 kcal/mol for MPO (Fig. 9G), and − 7.7 kcal/mol for RETN (Fig. 9H). These binding energies indicate strong and energetically favorable interactions between these drugs and the key proteins.

Discussion

The primary aim of this study was to unravel the molecular mechanisms driving AECOPD with *P. aeruginosa* infection through an integrative multi-omics approach. By combining proteomic analyses of BALF and plasma with transcriptomic profiling of peripheral blood, we sought to provide a comprehensive view of both local lung-specific responses and systemic immune activation. This approach has allowed us to identify key differentially expressed proteins and genes involved in the disease process. Our findings not only enhance the understanding of the pathogenesis of AECOPD with *P. aeruginosa* infection but also highlight potential biomarkers and therapeutic targets, which could lead to improved strategies for managing and treating the condition.

Functional enrichment analyses provided deeper insights into the biological processes and pathways associated with these key proteins. GO analysis revealed significant enrichment in processes such as defense response to bacteria, oxidative stress management, and neutrophil activity. These findings align with previous studies showing that neutrophils play a central role in the pathogenesis of AECOPD with *P. aeruginosa* infection by contributing to chronic inflammation and tissue damage through the release of proteases and reactive oxygen species [24, 25]. The KEGG pathway analysis further highlighted critical pathways, including neutrophil extracellular trap formation, emphasizing the central role of neutrophils in mediating immune responses and pathogen clearance in AECOPD with *P. aeruginosa* infection. While significant pathways were identified, the relatively low small sample sizes in some categories suggest caution in interpreting these findings, especially in complex diseases like COPD. To mitigate this limitation, we employed stringent statistical methods and corrections, including false discovery rate (FDR) adjustments, to reduce the likelihood of false positives in the enrichment analyses. Additionally, we cross-validated key findings with external datasets and performed validation in an independent cohort, thereby increasing confidence in the biological significance of our results.

The integrative analysis combining BALF, plasma and peripheral blood underscores the significance of local and systemic responses in AECOPD with *P. aeruginosa* infection. Identifying both lung-specific and blood-specific targets provides a comprehensive view of the disease's molecular landscape. The overlap of targets between BALF and plasma datasets highlight the coordinated immune response across different biological compartments. This systemic cross-talk suggests that the identified proteins may serve as biomarkers for diagnosis and potential therapeutic targets. At the same time, we focus on exploring therapeutic targets in the lungs by discovering and validating the BALF in the cohort. Among the identified proteins, Azurocidin 1 (AZU1), Myeloperoxidase (MPO), and Resistin (RETN) emerged as central players in the host defense mechanisms. AZU1 is stored in neutrophil granules and exhibits potent antimicrobial properties, including the ability to attract immune cells to sites of infection [26, 27]. The upregulation of AZU1 in AECOPD with *P. aeruginosa* infection suggests its involvement in reinforcing the innate immune response. MPO, an enzyme found abundantly in neutrophils, generates reactive oxygen species essential for bacterial killing [28, 29]. Elevated MPO levels in AECOPD with *P. aeruginosa* infection patients highlight the critical role of oxidative stress and neutrophil activation in the pathogenesis of the disease. RETN, a cytokine associated with inflammation and metabolic regulation [30, 31], was also significantly upregulated in COPD P.A. group, indicating its potential role in linking metabolic disturbances and inflammatory responses in AECOPD with *P. aeruginosa* infection patients. Although the expression for some

DEPs and DEGs were relatively low, the identification of these biomarkers in multiple datasets lends greater confidence to their biological relevance.

It is true that there are currently no well-established biomarkers specifically for AECOPD with *P. aeruginosa* infection, which is a key innovation of our study. The identified proteins—AZU1, MPO, and RETN—demonstrated strong diagnostic value, with AUC values of 0.830, 0.730, and 0.912, respectively. These findings underscore their potential as robust biomarkers for distinguishing AECOPD with *P. aeruginosa* infection from healthy controls. Compared to conventional inflammatory markers such as CRP and PCT, which are generally associated with broader inflammation but lack specificity for pathogen-induced exacerbations [32], AZU1, MPO, and RETN are more directly involved in bacterial defense and immune regulation in the context of AECOPD with *P. aeruginosa* infection.

Peroxisome proliferator-activated receptors (PPARs) hold significant promise as therapeutic agents for treating lung inflammation [33, 34]. In particular, PPARγ ligands can inhibit the release of proinflammatory cytokines from airway epithelial cells [35]. Beyond their well-established anti-inflammatory actions, PPAR agonists play a crucial role in the resolution phase of inflammation, a process vital for restoring tissue homeostasis [36]. This phase involves not only the suppression of proinflammatory signals but also actively promotes reparative and restorative processes in inflamed tissues. PPARγ agonists contribute to the resolution of inflammation through multiple mechanisms. They promote the polarization of macrophages towards the M2 phenotype, which are anti-inflammatory and essential for tissue repair and the resolution of inflammation [37]. Furthermore, PPARγ agonists modulate the recruitment of immune cells to sites of inflammation by regulating the expression of adhesion molecules and chemokines, thereby influencing the immune cell population towards an anti-inflammatory environment [38]. Noteworthy examples are Pioglitazone and Rosiglitazone, PPARγ agonists known not only for their roles in maintaining glucose and lipid homeostasis but also for their capacity to attenuate airway inflammation [39].

A study showed that Pioglitazone alleviates acute lung injury induced by lipopolysaccharide (LPS) by reducing the recruitment and activation of neutrophils [40]. Furthermore, Pioglitazone possesses potent anti-inflammatory properties, inhibiting the activation of nucleotide oligomerization-like receptor protein 3 (NLRP3) inflammasomes and ferroptosis [41], thus demonstrating its potential therapeutic benefits in pulmonary disorders. In COPD, alveolar macrophages exhibit a skewed M2 phenotype, and treatment with Rosiglitazone inhibits LPS-induced TNF-α and CCL-5 production [42]. It also increased the expression of CD36, HO-1, and PPARγ, key elements in the phagocytosis of apoptotic neutrophils and the resolution of inflammation [43]. In a subchronic tobacco smoke mouse model, rosiglitazone significantly reduced inflammatory cells in bronchoalveolar lavage, further illustrating its role in resolving pulmonary inflammation [44]. Molecular docking is a widely recognized and accepted method in drug discovery, frequently used to predict drug-target interactions and guide further experimental studies [45, 46]. Our study's molecular docking simulations demonstrated strong binding affinities of Pioglitazone and Rosiglitazone with key proteins identified in our analysis, suggesting their ability to modulate inflammatory pathways and oxidative stress. This understanding not only sheds light on the potential therapeutic applications of Pioglitazone and Rosiglitazone in managing AECOPD with *P. aeruginosa* infection but also unveils the underlying molecular mechanisms that govern these therapeutic effects.

This study has several limitations. The cross-sectional design inherently limits our ability to establish temporal relationships or causality between *P. aeruginosa* infection and the observed molecular changes. While our study identifies associations between AECOPD with *P. aeruginosa* infection and molecular alterations, it does not allow us to draw definitive cause-and-effect conclusions. Furthermore, although the primary focus was on AECOPD with *P. aeruginosa* infection, it is important to acknowledge that some of the observed molecular changes may also be influenced by COPD alone or AECOPD without *P. aeruginosa* infection. Nevertheless, we have made efforts to minimize the impact of pathogen-related variability on AECOPD, though the findings may not fully represent the specific molecular alterations driven by *P. aeruginosa* in COPD exacerbations. Additionally, COPD is a highly heterogeneous condition, and the observed immune responses may differ across patient subgroups [47, 48]. Future studies should consider stratifying patients based on comorbidities and infection status to refine therapeutic strategies. Lastly, while the multi-omics approach provided a comprehensive view of the molecular landscape, the integration of such diverse datasets requires careful consideration of batch effects and technical variability, which could influence the detection of low-abundance proteins.

Despite these limitations, our study provides valuable insights into the molecular mechanisms underlying AECOPD with *P. aeruginosa* infection. By integrating BALF, plasma, and peripheral blood data, we identified key proteins involved in oxidative stress and NET formation that are pivotal in disease progression. These findings improve the management of AECOPD with *P. aeruginosa* infection. Furthermore, we advocate for extending this research to AECOPD patients with other

bacterial pathogens to broaden the applicability of our conclusions and enhance the generalizability of these findings across different infection profiles.

Conclusion

This study utilized a multi-omics approach to elucidate the molecular mechanisms underlying AECOPD with *P. aeruginosa* infection, integrating proteomic analysis of BALF and plasma with transcriptomic analysis of peripheral blood. We identified three key proteins (AZU1, MPO, and RETN) highlighting their roles in oxidative stress and NETs formation, which are pivotal in the disease process. These proteins demonstrated significant diagnostic value and strong interactions with the therapeutic agent Pioglitazone and Rosiglitazone. The integration of local and systemic analyses provided a holistic view, revealing how pulmonary infections lead to systemic effects. Our findings advance the understanding of AECOPD with *P. aeruginosa* infection and suggest potential biomarkers and therapeutic targets, paving the way for improved diagnosis and treatment strategies.

Abbreviations

AECOPD	Acute Exacerbations of Chronic Obstructive Pulmonary Disease
BALF	Bronchoalveolar Lavage Fluid
COPD	Chronic Obstructive Pulmonary Disease
CRP	C-Reactive Protein
DIA	Data-Independent Acquisition
DEGs	Differentially Expressed Genes
DEPs	Differentially Expressed Proteins
DSigDB	Drug Signature Database
DTT	Dithiothreitol
FDR	False Discovery Rate
FEV1	Forced Expiratory Volume in one second
FVC	Forced Vital Capacity
GO	Gene Ontology
GOLD	Global Initiative for Chronic Obstructive Lung Disease
IAA	Iodoacetamide
LCN2	Lipocalin-2
LPS	Lipopolysaccharide
LYM	Lymphocyte
MCC	Maximum Clique Centrality
MCODE	Molecular Complex Detection
MONO	Monocyte
MPO	Myeloperoxidase
MS	Mass Spectrometry
NEU	Neutrophil
NETs	Neutrophil Extracellular Traps
NLRP3	Nucleotide oligomerization-like receptor protein 3
PASEF	Parallel Accumulation–Serial Fragmentation
PCT	Procalcitonin
PDB	Protein Data Bank
PPI	Protein-Protein Interaction
PPAR	Peroxisome Proliferator-Activated Receptor
RETN	Resistin
ROC	Receiver Operating Characteristic
ROS	Reactive Oxygen Species
SPSS	Statistical Package for the Social Sciences
STRING	Search Tool for the Retrieval of Interacting Genes/Proteins
TOM	Topological Overlap Matrix
UniProtKB	Universal Protein Resource Knowledgebase
WBC	White Blood Cell
WGCNA	Weighted Gene Co-Expression Network Analysis

Supplementary Information

The online version contains supplementary material available at https://doi.org/10.1186/s12931-025-03185-x.

Supplementary Material 1: Additional files 1: Supplementary Methods 1–6. Subject inclusion criteria, sample collection methods and multi-omics methodology supplement.

Supplementary Material 2: Additional files 2: Table S1-S2. Clinical data of the COPD P.A. group compared in the discovery cohort and validation cohort, and the control group compared in the discovery cohort and validation cohort.

Supplementary Material 3: Additional files 3: Supplementary Figures. Supplementary Figure S1-S2.

Supplementary Material 4: Additional files 4: Dataset 1–27. The original data and analysis results mentioned in the paper.

Acknowledgements

The authors would like to express their gratitude to Yaqin Li (Guangdong University of Foreign Studies) for the expert linguistic services provided. We thank the Immunology Department of the First Affiliated Hospital of Guangzhou Medical University for providing the experimental environment.

Author contributions

Zhiwei Lin and Shuang Liu should be regarded as co-first authors. Conception and design of the research: Luqian Zhou, Baoqing Sun. Drafting the manuscript: Zhiwei Lin and Luqian Zhou. Article structure design: Zhiwei Lin and Shuang Liu; Statistical analysis: Zhiwei Lin and Shuang Liu; Samples collection and detection: Shuang Liu and Tianyu Feng; Acquisition of data: Ke Zhang, Yue Xi and Hang Jiang; Experimental management: Zhiwei Lin and Luqian Zhou. All authors read and approved the final version of the manuscript.

Funding

National Key Research and Development Program of China (No.2023YFF1203802), Natural Science Foundation of Guangdong Province (No.2023A1515012917), Natural Science Foundation of Guangdong Province (No.2024A1515012830), State Key Laboratory Project (SKLRD-Z-202305), Research enhancement project of Guangzhou Medical University (No.2024SRP074).

Data availability

No datasets were generated or analysed during the current study.

Declarations

Ethics approval and consent to participate

Ethical approval for the inclusion of human subjects was granted by the Ethics Committee of The First Affiliated Hospital of Guangzhou Medical University, with approval codes 2022 No.121 and 2024 No. G-007. Written informed consent was secured from all study participants prior to their inclusion in the research.

Consent for publication

Not applicable.

Competing interests

The authors declare no competing interests.

Author details

[1]Respiratory Mechanics Laboratory, State Key Laboratory of Respiratory Disease, National Center for Respiratory Medicine, National Clinical Research Center for Respiratory Disease, Guangzhou Institute of Respiratory Health, Guangzhou 510120, China
[2]Department of Clinical Laboratory, Guangzhou Institute of Respiratory Health, State Key Laboratory of Respiratory Disease, National Center for Respiratory Medicine, National Clinical Research Center for Respiratory Disease, Guangzhou Laboratory, The First Affiliated Hospital of Guangzhou Medical University, Guangzhou 510120, China

[3]The First Clinical Medical School, Guangzhou Medical University, Guangzhou 510000, China

Received: 23 July 2024 / Accepted: 10 March 2025
Published online: 26 March 2025

References

1. Christenson SA, Smith BM, Bafadhel M, et al. Chronic obstructive pulmonary disease. Lancet. 2022;399(10342):2227–42.
2. Brennan M, McDonnell M, Harrison M et al. Antimicrobial therapies for prevention of recurrent acute exacerbations of COPD (AECOPD): beyond the guidelines. Respir Res. 2022;23(1):58.
3. Aaron SDJB. *Management and prevention of exacerbations of COPD.* 2014. 349.
4. Hurst JR, Anzueto A, J.J.T.L.R M, Vestbo. Susceptibility Exacerbation COPD. 2017;5(9):e29.
5. Biancardi E, Fennell M, Rawlinson W et al. Viruses are frequently present as the infecting agent in acute exacerbations of chronic obstructive pulmonary disease in patients presenting to hospital. Intern Med J. 2016;46(10):1160–5.
6. Moghoofei M, Azimzadeh Jamalkandi S, Moein M et al. Bacterial infections in acute exacerbation of chronic obstructive pulmonary disease: a systematic review and meta-analysis. Infection. 2020;48(1):19–35.
7. Wilson R, Sethi S, Anzueto A, et al. Antibiot Treat Prev Exacerbations Chronic Obstr Pulmonary Disease. 2013;67(6):497–515.
8. Riquelme SA, Prince AJRr. Airw Immunometabolites Fuel Pseudomonas aeruginosa Infect. 2020;21(1):326.
9. Erb-Downward JR, Thompson DL, Han MK, et al. Anal Lung Microbiome Healthy Smoker COPD. 2011;6(2):e16384.
10. Qin S, Xiao W, Zhou C et al. Pseudomonas aeruginosa: pathogenesis, virulence factors, antibiotic resistance, interaction with host, technology advances and emerging therapeutics. Signal Transduct Target Ther. 2022;7(1):199.
11. Vareechon C, Zmina SE, Karmakar M et al. Pseudomonas aeruginosa effector exos inhibits ROS production in human neutrophils. Cell Host Microbe. 2017;21(5):611–8.e5.
12. Yang S-C, Tsai Y-F, Pan Y-L, et al. Understanding the role of neutrophils in acute respiratory distress syndrome. Biomedical J. 2021;44(4):439–46.
13. Hidalgo A, Libby P, Soehnlein O, et al. Neutrophil Extracell Traps: Physiol Pathol. 2022;118(13):2737–53.
14. Castanheira FV, Kubes PJB. Neutrophils and NETs in modulating acute and chronic inflammation. J Am Soc Hematol. 2019;133(20):2178–85.
15. Zlatar L, Mahajan A, Muñoz-Becerra M, et al. Suppression Neutrophils Sodium Exacerbates Oxidative Stress Arthritis. 2023;14:1174537.
16. Langfelder P, Horvath SJBb. WGCNA: R Package Weighted Correlation Netw Anal. 2008;9:1–13.
17. Yoo M, Shin J, Kim J, et al. DSigDB: Drug Signatures Database Gene Set Anal. 2015;31(18):3069–71.
18. Xing X, Cai L, Ouyang J, et al. Proteomics-driven noninvasive screening of Circulating serum protein panels for the early diagnosis of hepatocellular carcinoma. Nat Commun. 2023;14(1):8392.
19. Collins BC, Hunter CL, Liu Y, et al. Multi-laboratory assessment of reproducibility, qualitative and quantitative performance of SWATH-mass spectrometry. Nat Commun. 2017;8(1):291.
20. Zhang B, Horvath S. A general framework for weighted gene co-expression network analysis. Stat Appl Genet Mol Biol, 2005. 4(1).
21. Sui S, An X, Xu C, et al. An immune cell infiltration-based immune score model predicts prognosis and chemotherapy effects in breast cancer. Theranostics. 2020;10(26):11938.
22. Tyanova S, Temu T, Sinitcyn P, et al. The perseus computational platform for comprehensive analysis of (prote) omics data. Nat Methods. 2016;13(9):731–40.
23. Davies MPA, Sato T, Ashoor H, et al. Plasma Protein Biomarkers Early Prediction Lung cancer EBioMedicine. 2023;93:104686.
24. Cheetham CJ, McKelvey MC, McAuley DF, et al. Neutrophil-Derived Proteases Lung Inflammation: Old Players New Prospects. 2024;25(10):5492.
25. Thind MK, Uhlig HH, Glogauer M et al. *A metabolic perspective of the neutrophil life cycle: new avenues in immunometabolism.* 2024. 14: p. 1334205.
26. Meng Y, Zhang L, Huang M et al. Blood heparin-binding protein and neutrophil-to-lymphocyte ratio as indicators of the severity and prognosis of community-acquired pneumonia. Respir Med. 2023;208:107144.
27. Aquino-Domínguez AS, Acevedo-Sánchez V, Cruz-Hernández DS et al. *Human Platelets Contain, Translate, and Secrete Azurocidin; A Novel Effect on Hemostasis.* 2022. 23(10): p. 5667.
28. Manoharan RR, Prasad A, Pospíšil P, et al. ROS Signal Innate Immun Via Oxidative Protein Modifications. 2024;15:1359600.
29. Lin W, Chen H, Chen X et al. *The Roles of Neutrophil-Derived Myeloperoxidase (MPO) in Diseases: The New Progress.* 2024. 13(1): p. 132.
30. Schwartz DR, M.A.J.T.i E, Lazar, Metabolism. Hum Resistin: Found Translation Mouse Man. 2011;22(7):259–65.
31. Sudan SK, Deshmukh SK, Poosarla T et al. *Resistin: An inflammatory cytokine with multi-faceted roles in cancer.* 2020. 1874(2): p. 188419.
32. Hoult G, Gillespie D, Wilkinson TMA, et al. Biomarkers to guide the use of antibiotics for acute exacerbations of COPD (AECOPD): a systematic review and meta-analysis. BMC Pulm Med. 2022;22(1):194.
33. Belvisi MG, Hele DJJC. Peroxisome proliferator-activated Receptors as Novel Targets Lung Disease. 2008;134(1):152–7.
34. Belvisi MG, J.A.J..B.j.o.p. Mitchell. Target PPAR Receptors Airw Treat Inflamm Lung Disease. 2009;158(4):994–1003.
35. Ryu SL, Shim JW, Kim DS et al. Expression of peroxisome proliferator-activated receptor (PPAR)-α and PPAR-γ in the lung tissue of obese mice and the effect of Rosiglitazone on Proinflammatory cytokine expressions in the lung tissue. Korean J Pediatr. 2013;56(4):151–8.
36. Lee KS, Park SJ, Hwang PH, et al. PPAR-gamma Modulates Allergic Inflamm Through up-regulation PTEN. 2005;19(8):1033–5.
37. Guyton K, Zingarelli B, Ashton S et al. Peroxisome proliferator-activated receptor-gamma agonists modulate macrophage activation by gram-negative and gram-positive bacterial stimuli. Shock. 2003;20(1):56–62.
38. Liu Y, Wang J, Luo S et al. *The roles of PPARγ and its agonists in autoimmune diseases: A comprehensive review.* 2020. 113: p. 102510.
39. Xu J, Zhu Y-t, Wang G-z et al. The PPARγ agonist, Rosiglitazone, attenuates airway inflammation and remodeling via Heme oxygenase-1 in murine model of asthma. Acta Pharmacol Sin. 2015;36(2):171–8.
40. Grommes J, Mörgelin M, Soehnlein O. Pioglitazone attenuates endotoxin-induced acute lung injury by reducing neutrophil recruitment. Eur Respir J. 2012;40(2):416–23.
41. Pan J, Wang Z, Huang X, et al. Bacteria-Derived Outer-Membrane vesicles hitchhike neutrophils to enhance ischemic stroke therapy. Adv Mater. 2023;35(38):e2301779.
42. Lea S, Plumb J, Metcalfe H et al. *The effect of peroxisome proliferator-activated receptor-γ ligands on in vitro and in vivo models of COPD.* 2014. 43(2): pp. 409–420.
43. Ballesteros I, Cuartero MI, Pradillo JM et al. Rosiglitazone-induced CD36 up-regulation resolves inflammation by PPARγ and 5-LO-dependent pathways. J Leukoc Biol. 2014;95(4):587–98.
44. Feng H, Yin Y, Zheng R et al. Rosiglitazone ameliorated airway inflammation induced by cigarette smoke via inhibiting the M1 macrophage polarization by activating PPARγ and RXRα. Int Immunopharmacol. 2021;97:107809.
45. Stoddard BL, Koshland DE Jr. Molecular recognition analyzed by Docking simulations: the aspartate receptor and isocitrate dehydrogenase from Escherichia coli. Proc Natl Acad Sci U S A. 1993;90(4):1146–53.
46. Huang S. Efficient analysis of toxicity and mechanisms of environmental pollutants with network toxicology and molecular Docking strategy: acetyl tributyl citrate as an example. Sci Total Environ. 2023;905:167904.
47. Wedzicha JJT. The heterogeneity of chronic obstructive pulmonary disease. BMJ Publishing Group Ltd; 2000. pp. 631–2.
48. Castaldi PJ, Benet M, Petersen H et al. Do COPD subtypes really exist? COPD heterogeneity and clustering in 10 independent cohorts. Thorax. 2017;72(11):998–1006.

Publisher's note